Donghyuk Kang
Assistant Professor
Mechanical Engineering,
Aoyama Gakuin University,
5-10-1 Fuchinobe, Chuo-ku,
Sagamihara 252-5258, Japan
e-mail: Kang@me.aoyama.ac.jp

Kazuhiko Yokota
Professor
Mem. ASME
Mechanical Engineering,
Aoyama Gakuin University,
5-10-1 Fuchinobe, Chuo-ku,
Sagamihara 252-5258, Japan
e-mail: Yokota@me.aoyama.ac.jp

Analytical Study of Cavitation Surge in a Hydraulic System

In order to clarify effects of an accumulator, pipe lengths and gradients of pressure and suction performances on cavitation surge, one-dimensional stability analyses of cavitation surge were performed in hydraulic systems consisting of an upstream tank, an inlet pipe, a cavitating pump, a downstream pipe, and a downstream tank. An accumulator located upstream or downstream of the cavitating pump was included in the analysis. Increasing the distance between the upstream accumulator and the cavitating pump enlarged the stable region. On the other hand, decreasing the distance between the downstream accumulator and the cavitating pump enlarged the stable region. Furthermore, the negative gradient of a suction performance curve and the positive gradient of a pressure performance curve cause cavitation surge. [DOI: 10.1115/1.4027220]

Keywords: cavitation surge, stability analysis, accumulator, gradient of suction performance curve

Introduction

Cavitation is usually observed in various turbomachines. Various cavitation instabilities are often observed in a range of cavitation numbers, which are higher than a degradation of a pump performance due to cavitation [1,2]. Cavitation instabilities may induce flow and pressure oscillations and result in a severe shaft vibration.

Cavitation instabilities are classified into two categories. One is generally called a "local instability," which is caused by the mutual interference between cavitation and an impeller, including "rotating cavitation," "alternate blade cavitation," and "asymmetric cavitation". The other is generally called a "system instability," which is caused by the mutual interference between cavitation and a hydraulic system, i.e., "cavitation surge" focused in the present study.

Two mechanisms of cavitation surge have been reported [3]. One is called a "positive mass flow gain factor" [4,5], which occurs when the cavity volume decreases with an increase in a flow rate. The destabilizing effects of the positive mass flow gain factor can be physically explained as follows. If the cavity volume decreases, the inlet flow rate increases, which causes the decrease of the cavity volume further due to the decrease of the incidence angle. This positive feedback causes cavitation surge [6]. The other mechanism is related to the cavitating pump performances. The cavitating pump performances are generally described by pressure and suction performance curves. The pressure performance curve is a relation between a total pressure rise and a flow rate at a constant cavitation number. The suction performance curve plots a total pressure rise versus a cavitation number at a constant flow rate.

Figure 1 shows the suction performance of a four-bladed inducer for various flow rates and the amplitude of the pressure oscillation [7]. At $\phi = 0.076$, we can observe the sudden pressure breakdown at higher cavitation numbers. In $0.015 < \sigma < 0.020$, the static pressure coefficient of $\phi = 0.077$ is larger than that of $\phi = 0.076$. That is, the gradient of the pressure performance curve in $0.015 < \sigma < 0.020$ has the positive value, i.e., "positive flow gain." The amplitude of the pressure oscillation with the frequency of 5 ~10 Hz is observed in $0.015 < \sigma < 0.020$, as shown at the bottom of Fig. 1. This result suggests that the gradient of the pressure performance curve can be changed due to cavitation and that the positive gradient of the pressure performance curve causes "choke surge."

Figure 2 shows the suction performance curve for an axial pump [8]. The auto oscillations considered as cavitation surge indicated by the star symbol are observed in lower cavitation numbers than $\sigma = 0.04$ in which the negative and positive gradients of the suction performance curve is observed due to cavitation. Thus, the gradient of the suction performance curve, i.e., "pressure gain," is closely related to the onset of cavitation surge. However, the effect of pressure gain on cavitation surge has not yet been clarified.

Several studies on the unsteady performance curves and the unsteady cavitation characteristics have been reported. Yamamoto [9] and Yamamoto and Tsujimoto [10] investigated the flow instabilities in a centrifugal cavitating pump, and it was found that the phase delay of the backflow vortex cavitation is closely related to cavitation surge. Kawata et al. [11] showed an example in which the negative gradient of the pressure performance curve under quasi-steady conditions becomes positive under unsteady conditions due to the phase delay. Brennen and Acosta [4], Otsuka et al. [12], Watanabe et al. [13], and Rubin [14] showed that the mass flow gain factor and the cavitation compliance have the phase delay under the unsteady conditions. Therefore, the unsteady characteristics of performance curves and cavitation characteristics are important to discuss the stability of the hydraulic system.

For the suppression of Pogo instabilities of liquid rockets, which is longitudinal vibration caused by the coupling of the thrust fluctuation, the structure vibration, and the fluctuation of propellant supply to the engine, an accumulator reducing the flow oscillation with minimal pressure rise has been installed in the hydraulic system [15]. However, the effect of the accumulator on cavitation surge has not yet been revealed.

The stability analysis of cavitation surge was firstly conducted by Tsujimoto et al. [16], with the assumption that the flow oscillation does not occur downstream of a cavitating pump and that the pressure rise is not changed due to cavitation. The onset condition of cavitation surge was given by $M > 2(1 + \sigma_u)\,\phi K$. That is, cavitation surge occurs when a mass flow gain factor M is larger than a certain value calculated from a cavitation number σ_u, a flow coefficient ϕ and a cavitation compliance K. Here, the mass flow gain factor M indicates the variation of the cavity to the inlet flow oscillation. The cavitation number σ_u shows how close the pressure in the liquid flow is to the vapor pressure. The cavitation compliance K implies the variation of the cavity to the inlet pressure oscillation.

In a cavitation surge of a real cavitating pump, an outlet flow oscillation was observed [10]. As shown in Figs. 1 and 2, at lower

Contributed by the Fluids Engineering Division of ASME for publication in the Journal of Fluids Engineering. Manuscript received June 2, 2013; final manuscript received March 17, 2014; published online July 24, 2014. Assoc. Editor: Daniel Maynes.

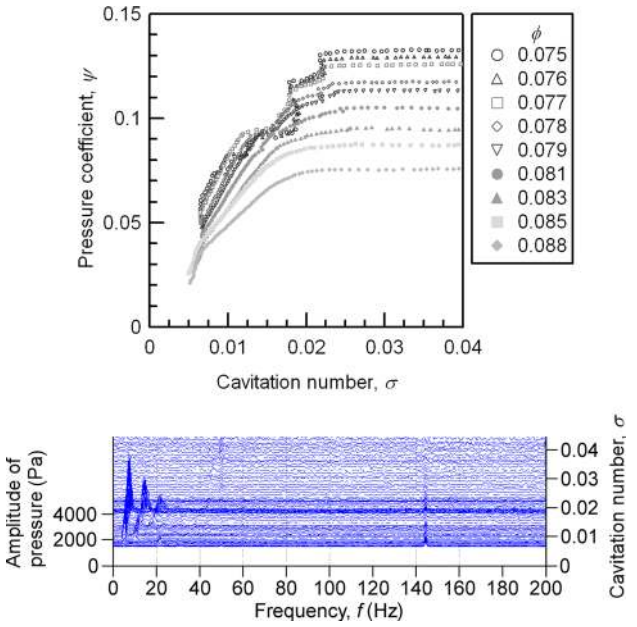

Fig. 1 Suction performance curve of four bladed inducer (upper) and the amplitude of pressure oscillation (bottom), from Watanabe et al. [7]

cavitation numbers, the changes of gradients of the suction and pressure performance curves appear due to cavitation. The effects of pressure rise due to cavitation and the outlet flow oscillation were not taken into account in the previous study.

In the present study, one-dimensional stability analyses of cavitation surge were performed with respect to three hydraulic systems. All systems consisted of an upstream tank, an inlet pipe, a cavitating pump, a downstream pipe, and a downstream tank, as shown in Fig. 3. The variation in the three systems was in the position of the accumulators. The first system does not have an accumulator as shown in Fig. 3(*a*), the second has an accumulator upstream of the cavitating pump as shown in Fig. 3(*b*), and the final system has an accumulator downstream of the cavitating pump as shown in Fig. 3(*c*). The pressure rise by cavitation was taken into account when evaluating the lumped-parameter of the cavitating pump.

For comparison of the analytical results with the experimental results, the mass flow gain factor and the cavitation compliance should be known. However, the quantitative evaluations of the cavitation compliance and the mass flow gain factor of real cavitating pumps are extremely difficult. Although few papers

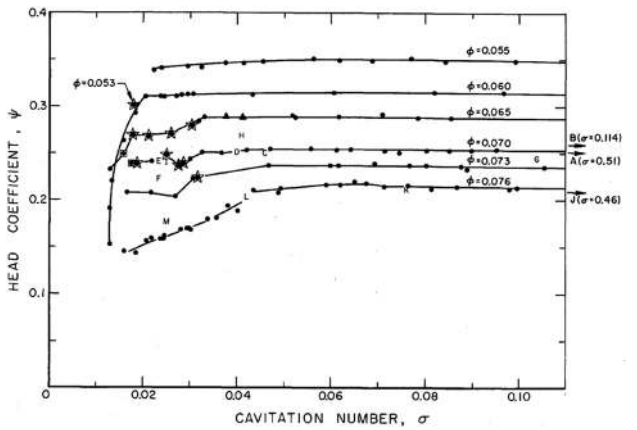

Fig. 2 Suction performance curve of impeller IV at 9000 rpm [8] with the amplitude of auto-oscillation indicated by ★

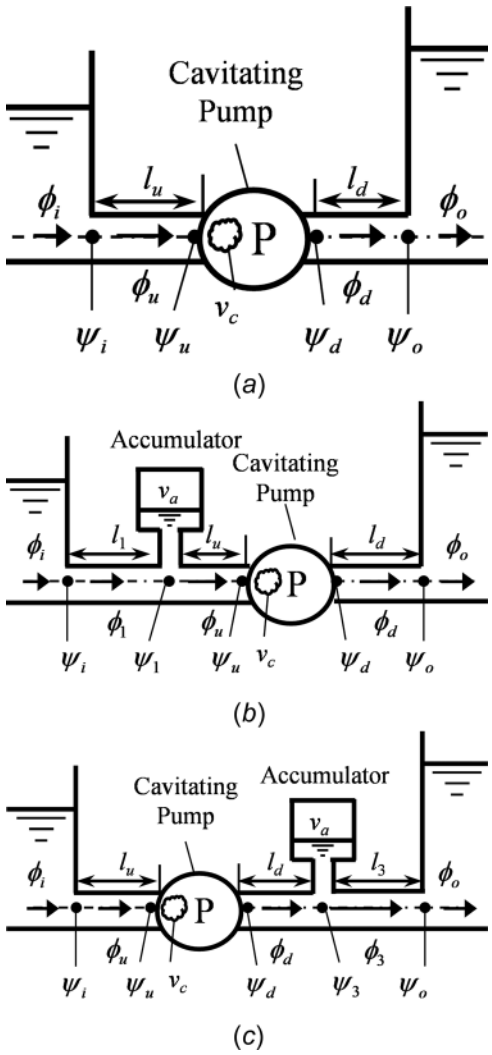

Fig. 3 Analytical model of cavitation surge in the hydraulic systems

[5,14,17] evaluating the mass flow gain factor and the cavitation compliance of real cavitating pumps exists, the reliable data is limited. Thus, we qualitatively discussed the effects of the accumulator, the pipe lengths, and the gradients of suction and pressure performance curves on cavitation surge within the range of the mass flow gain factor and the cavitation compliance shown in the experiments [5,14,17].

Table 1 shows the analytical parameters determined by considering test facilities at Osaka University [2]. These parameters are used in the present paper as the default parameters.

Table 1 Default analytical parameters

Tip diameter (mm), D	150.8
Tip velocity (m/s), U	23.5
Dimensionless inlet pipe length, l_u	10
Dimensionless chord length, l_p	0.3
Dimensionless outlet pipe length, l_d	100
Flow rate, $\bar{\phi}$	0.1
Inlet and outlet loss coefficients, λ_u, λ_d	0.01
Flow gain, R_p	−3
Pressure gain, S_p	0
Dimensionless compliance of accumulator, c	100
Density of working fluid (kg/m^3), ρ	997

Analytical Method

The dynamics of hydraulic systems were treated in terms of lumped-parameter models [18], which simplifies the description of the physical effects between two measuring sections. The lumped-parameter model is usually considered valid when the dimensions of a hydraulic system are shorter than the acoustic wavelength at the considered frequency. For simplicity of the analytical model, the following assumptions are adopted in the present analysis.

(1) The flow is one-dimensional.
(2) The flow oscillations are expressed as a temporally harmonic oscillation and infinitesimal. The second or higher order quantities, therefore, are negligible.
(3) The working fluid is incompressible. The pressure loss is considered as the loss coefficient.
(4) The elastic deformation of all pipes is negligible and the cross-sectional area of the pipe is constant.
(5) The potential energy of the fluid is negligible.
(6) The compliance of a tank is large and, thus, the pressure oscillation inside tanks is negligible.

Under the above assumptions, the dimensionless pressure oscillation and the dimensionless flow oscillations can be written in the complex form as follows:

$$\psi(t) = \bar{\psi} + \hat{\psi}e^{j\omega t}, \phi(t) = \bar{\phi} + \hat{\phi}e^{j\omega t} \tag{1}$$

Here, $\bar{\psi} = \bar{p}/\rho U^2$ and $\bar{\phi} = \bar{Q}/AU$ are the steady pressure coefficient and the steady flow coefficient. $\hat{\psi} = \hat{p}/\rho U^2$ and $\hat{\phi} = \hat{Q}/AU$ are the complex amplitudes of the unsteady pressure coefficient and the unsteady flow coefficient. $t = \tau \times U/D$ and $\omega = \Omega \times D/U$ are the dimensionless time and the dimensionless complex angular frequency. A and D are the cross-sectional area and the diameter of the pipe. Ω and U are the angular velocity and the tip velocity of an impeller. ρ is the density of the working fluid. j is the imaginary unit.

Consider the flow through the inlet pipe shown in Fig. 3(*a*). By putting Eq. (1) into the dimensionless unsteady continuity equation and the dimensionless unsteady momentum equation and subtracting the steady terms of them from themselves, the following equations can be introduced:

$$\hat{\phi}_i = \hat{\phi}_u \tag{2}$$

$$\hat{\psi}_u = -\lambda_u l_u \bar{\phi}\hat{\phi}_u - j\omega l_u \hat{\phi}_u \tag{3}$$

Here, superscripts i and u indicate the inlet tank and the inlet pipe, respectively. λ is the loss coefficient. $l = L/D$ is the dimensionless pipe length. The first and second terms of the right side in Eq. (3) indicates the hydraulic resistance and the hydraulic inertance, respectively.

Next, we consider the flow through the accumulator shown in Fig. 3(*b*). The fluid inside the accumulator tank is assumed to be an isentropic fluid and then the flow through the accumulator can be expressed as

$$\hat{\phi}_u - \hat{\phi}_1 = -j\omega \frac{v_a}{\gamma\bar{\psi}_1}\hat{\psi}_1 = -cj\omega\hat{\psi}_1 \tag{4}$$

Here, $v_a = V_a/AD$ is the dimensionless fluid volume at the top of the accumulator. γ is the specific heat ratio of the fluid at the top of the accumulator, and c is the compliance of the accumulator.

A cavity volume V_c is assumed to be formed upstream of the cavitating pump. Then, the dimensionless continuity equation can be expressed as

$$\phi_d(t) - \phi_u(t) = \frac{dv_c(t)}{dt} \tag{5}$$

Here, $v_c = V_c/AD$ is the dimensionless cavity volume. The change of the cavity volume dv_c can be considered to be functions of the upstream cavitation number $\sigma_u = 2(p_u - p_v)/\rho U^2$ and the upstream flow coefficient $\phi_u = Q_u/AU$. Thus, it can be written as

$$dv_c = \left(\left.\frac{\partial v_c}{\partial \phi_u}\right|_{\sigma_u} d\phi_u + \left.\frac{\partial v_c}{\partial \sigma_u}\right|_{\phi_u} d\sigma_u\right) = (-Md\phi_u - Kd\sigma_u) \tag{6}$$

where M and K are the mass flow gain factor and the cavitation compliance, respectively. By putting Eqs. (1) and (6) in Eq. (5), the following equation yields:

$$\hat{\phi}_d = -j\omega 2K\hat{\psi}_u + (1 - j\omega M)\hat{\phi}_u \tag{7}$$

The pressure rise supplied from the cavitating pump can be expressed as the total pressure rise coefficient. The total pressure rise coefficient is defined as

$$\psi_p = (p_{td} - p_{tu})/\rho U^2 \tag{8}$$

Here, p_{tu} and p_{td} are the total pressures upstream of the cavitating pump and downstream of the cavitating pump, respectively. The unsteady pressure rise can be expressed as

$$\hat{\psi}_d - \hat{\psi}_u = \hat{\psi}_p - \bar{\phi}\left(\hat{\phi}_d - \hat{\phi}_u\right) - j\omega l_p \hat{\phi}_d \tag{9}$$

Here, $l_p = L_p/D$ is the dimensionless inertial length of the cavitating pump. L_p is the mean value of the chord length of an impeller. The first term of the right side indicates the unsteady total pressure rise of the cavitating pump. The second term of the right side shows the unsteady dynamic pressure rise. The last term of the right side is caused by the inertia due to the discharge flow oscillation. $\hat{\psi}_p$ can be considered to be functions of the upstream cavitation number σ_u and the discharge flow coefficient ϕ_d on the assumption that cavitation occurs upstream of a cavitating pump and that the total pressure rise depends on the discharge flow rate. Thus, we can represent the unsteady pressure rise as

$$\hat{\psi}_p = \left(\left.\frac{\partial \psi_p}{\partial \phi_d}\right|_{\sigma_u} \hat{\phi}_d + \left.\frac{\partial \psi_p}{\partial \sigma_u}\right|_{\phi_d} \hat{\sigma}_u\right) = \left(R_p\hat{\phi}_d + 2S_p\hat{\psi}_u\right) \tag{10}$$

Here, R_p and S_p are flow gain and pressure gain, respectively. In the present study, the influences of these parameters on cavitation surge will be examined.

From above formulations, we obtained the homogeneous linear equations for each analytical model tested in the present research. The analytical model without the accumulator can be expressed as the third-order homogeneous linear equation written as

$$\begin{aligned}
&B_{a3}\omega^3 + B_{a2}\omega^2 + B_{a1}\omega + B_{a0} = 0\\
&B_{a3} = 2Kl_d l_u j + 2KL_p l_u j\\
&B_{a2} = l_d(-M + 2K\bar{\phi}l_u\lambda_u) + l_p(-M + 2K\bar{\phi}l_u\lambda_u) + 2\bar{\phi}Kl_u\\
&\quad - 2KR_p l_u + 2\bar{\phi}Kl_d\lambda_d l_u)\\
&B_{a1} = (-l_d j - l_p j - l_u j + \bar{\phi}(Mj - 2K\bar{\phi}l_u\lambda_u j)\\
&\quad - R_p(Mj - 2K\bar{\phi}l_u\lambda_u j)\\
&\quad - 2S_p l_u j + \bar{\phi}l_d\lambda_d(Mj - 2K\bar{\phi}l_u\lambda_u j))\\
&B_{a0} = R_p - 2S_p\bar{\phi}l_u\lambda_u - 2\bar{\phi}l_d\lambda_d - 2\bar{\phi}l_u\lambda_u
\end{aligned} \tag{11}$$

The third-order homogeneous linear equation has the three dimensionless complex angular frequencies $\omega_1 = \omega_{1R} + j\omega_{1I}$, $\omega_2 = -\omega_{1R} + j\omega_{1I}$, $\omega_3 = j\omega_{3I}$. ω_R and ω_I show the angular frequency and the damping rate, respectively. ω_1 and ω_2 are the one pair solution of cavitation surge and ω_3 is the divergence solution. On the other hand, the analytical models with the upstream and

downstream accumulators can be expressed as the fifth-order homogeneous linear equations written as

$$
\begin{aligned}
&B_{b5}\omega^5 + B_{b4}\omega^4 + B_{b3}\omega^3 + B_{b2}\omega^2 + B_{b1}\omega + B_{b0} = 0\\
&B_{b5} = -2l_1c(Kl_dl_uj + Kl_pl_uj)\\
&B_{b4} = (l_p(2K(-\bar{\phi}l_1l_u\lambda_1c - \bar{\phi}l_1l_u\lambda_uc) + l_1Mc) - 2\bar{\phi}Kl_1l_uc\\
&\quad + 2Kl_1l_uR_pc - 2\bar{\phi}Kl_1l_dl_u\lambda_dc + l_d(2K(-\bar{\phi}l_1l_u\lambda_1c - \bar{\phi}l_1l_u\lambda_uc)\\
&\quad + l_1Mc)\\
&B_{b3} = \bar{\phi}(2K(\bar{\phi}l_1l_u\lambda_1c + \bar{\phi}l_1l_u\lambda_uc)j - l_1Mcj) - R_p(2K(\bar{\phi}Kl_1l_u\lambda_1c\\
&\quad + \bar{\phi}Kl_1l_u\lambda_uc)j - l_1Mcj) - l_d(-l_1c - 2K(\bar{\phi}^2l_1l_u\lambda_1\lambda_uc + l_u)\\
&\quad + \bar{\phi}l_1M\lambda_1c)j - l_p(-l_1c - 2K(\bar{\phi}^2l_1l_u\lambda_1\lambda_uc + l_u)\\
&\quad + \bar{\phi}l_1M\lambda_1c)j + l_1l_ucj + 2l_1l_uS_pcj + \bar{\phi}l_d\lambda_d(2K(\bar{\phi}l_1l_u\lambda_1c\\
&\quad + \bar{\phi}l_1l_u\lambda_uc)j - l_1Mcj))\\
&B_{b2} = -\bar{\phi}(2K(-\bar{\phi}^2l_1l_u\lambda_1\lambda_uc - l_u) + \bar{\phi}l_1M\lambda_1c)\\
&\quad + R_p(-l_1c + 2K(-\bar{\phi}^2l_1l_u\lambda_1\lambda_{u1}c - l_u) + \bar{\phi}l_1M\lambda_1c)\\
&\quad - l_d(M - 2\bar{\phi}Kl_u\lambda_u - \bar{\phi}l_1\lambda_1c) - l_p(M - 2\bar{\phi}Kl_u\lambda_u - \bar{\phi}l_1\lambda_1c)\\
&\quad + 2S_p(\bar{\phi}l_1l_u\lambda_1c + \bar{\phi}l_1l_u\lambda_uc) - \bar{\phi}l_d\lambda_d(-l_1c - 2K(\bar{\phi}^2l_1l_u\lambda_1c\\
&\quad + l_u) + \bar{\phi}l_1M\lambda_1c) + \bar{\phi}l_1l_u\lambda_1c + \bar{\phi}l_1l_u\lambda_uc)\\
&B_{b1} = (-l_dj - l_pj - l_uj + \bar{\phi}(Mj - 2K\bar{\phi}l_u\lambda_uj)\\
&\quad - 2S_p(\bar{\phi}^2l_1l_u\lambda_1\lambda_ucj + l_uj) + R_p(-Mj + 2\bar{\phi}Kl_u\lambda_uj + \bar{\phi}l_1\lambda_1cj)\\
&\quad - \bar{\phi}l_d\lambda_d(-Mj + 2K\bar{\phi}l_u\lambda_uj + \bar{\phi}l_1\lambda_1cj) - \bar{\phi}^2l_1l_u\lambda_1\lambda_ucj)\\
&B_{b0} = R_p - \bar{\phi}l_d\lambda_d - \bar{\phi}l_u\lambda_u - 2\bar{\phi}l_u\lambda_uS_p
\end{aligned}
\tag{12}
$$

and

$$
\begin{aligned}
&B_{c5}\omega^5 + B_{c4}\omega^4 + B_{c3}\omega^3 + B_{c2}\omega^2 + B_{c1}\omega + B_{c0} = 0\\
&B_{c5} = -2l_2c(Kl_dl_uj + Kl_pl_uj)\\
&B_{c4} = (-l_2c(l_p(-M + 2\bar{\phi}Kl_u\lambda_u) + 2\bar{\phi}Kl_u - 2Kl_uR_p + 2\bar{\phi}Kl_dl_u\lambda_d\\
&\quad + l_d(-M + 2\bar{\phi}Kl_u\lambda_u)) + \bar{\phi}l_2\lambda_2c(-2Kl_dl_u - 2Kl_pl_u))\\
&B_{c3} = -l_2(-2Kl_u + c(l_dj + l_pj + l_uj - \bar{\phi}(Mj - 2\bar{\phi}Kl_u\lambda_uj)\\
&\quad + R_p(Mj - 2\bar{\phi}Kl_u\lambda_uj) + 2l_uS_pj - \bar{\phi}l_d\lambda_d(-M + 2\bar{\phi}Kl_u\lambda_u))j\\
&\quad + 2Kl_dl_uj + 2Kl_pl_uj + \bar{\phi}l_2\lambda_2c(l_p(-M + 2\bar{\phi}Kl_u\lambda_u) + 2\bar{\phi}Kl_u\\
&\quad - 2Kl_uR_p + 2\bar{\phi}Kl_dl_u\lambda_d + l_d(-M + 2\bar{\phi}Kl_u\lambda_u))j\\
&B_{c2} = -l_2(M - c(\bar{\phi}l_d\lambda_d - R_p + \bar{\phi}l_u\lambda_u + 2\bar{\phi}l_u\lambda_uS_p) - 2\bar{\phi}Kl_u\lambda_u)\\
&\quad + l_d(-M + 2\bar{\phi}Kl_u\lambda_u) + l_p(-M + 2\bar{\phi}Kl_u\lambda_u) + 2\bar{\phi}Kl_u\\
&\quad - 2Kl_uR_p - \bar{\phi}l_2R_2(-2Kl_u + c(-l_d - l_p - l_u\\
&\quad - \bar{\phi}(-M + 2\bar{\phi}Kl_u\lambda_u) + R_p(-M + 2\bar{\phi}Kl_u\lambda_u) - 2l_uS_p\\
&\quad - \bar{\phi}l_d\lambda_d(-M + 2\bar{\phi}Kl_u\lambda_u)) + 2\bar{\phi}Kl_dl_u\lambda_d\\
&B_{c1} = (-l_2j - l_dj - l_pj - l_uj + \bar{\phi}(Mj - 2K\bar{\phi}l_u\lambda_uj)\\
&\quad - R_p(Mj - 2\bar{\phi}Kl_u\lambda_uj) - 2S_pl_uj - \bar{\phi}l_2\lambda_2(-Mj + c(\bar{\phi}l_d\lambda_d\\
&\quad - R_p + \bar{\phi}l_u\lambda_u + 2\bar{\phi}l_u\lambda_uS_p)j + 2\bar{\phi}Kl_u\lambda_uj)\\
&\quad + \bar{\phi}l_d\lambda_d(Mj - 2K\bar{\phi}l_u\lambda_uj))\\
&B_{c0} = R_p - \bar{\phi}l_2\lambda_2 - \bar{\phi}l_d\lambda_d - \bar{\phi}l_u\lambda_u - S_p\bar{\phi}l_u\lambda_u
\end{aligned}
\tag{13}
$$

respectively. The fifth-order homogeneous linear equations have the one pair solution of cavitation surge, the one pair solution of normal surge, and the divergence solution. In the present study, the one pair solution of cavitation surge will be mainly discussed.

Results and Discussion

Influence of the Inlet Pipe Length. For the further simplicity of the analytical model without the accumulator shown in Fig. 3(*a*), we assumed that the flow oscillation does not occur downstream of a cavitating pump $\hat{\phi}_d = 0$. This would be the case if there is a very long conduit or a large resistance existing downstream of a cavitating pump. By using Eqs. (3) and (7), we obtain the second-order linear formulation as

$$
l_u\omega^2 + \left[\frac{M}{2K} - \bar{\phi}\lambda_ul_u\right]j\omega - \frac{1}{2K} = 0 \tag{14}
$$

Here, the first, second, and third terms correspond to the mass, damping, and stiffness coefficients, respectively. If the damping coefficient has the negative value, the infinitesimal magnitudes of the pressure and flow oscillations shown in Eq. (1) becomes infinite, which indicates that cavitation surge occurs. The angular velocity at the onset condition of cavitation surge is identical to the undamped natural frequency of Eq. (14). Thus, the onset condition of cavitation surge and its angular frequency can be analytically obtained as

$$
M > 2K\bar{\phi}\lambda_ul_u \tag{15}
$$

$$
\omega_R = \sqrt{\frac{1}{2Kl_u}} \tag{16}
$$

These solutions show that cavitation surge occurs when the mass flow gain factor is larger than the certain value and that the angular frequency is evaluated from the cavitation compliance and the inlet pipe length. The onset condition of cavitation surge and its angular frequency are qualitatively the same as the results of the reference [16].

Figure 4 shows the stability map of cavitation surge for various inlet pipe lengths. The horizontal and vertical axes show the mass flow gain factor and the cavitation compliance, respectively. The very long outlet pipe $l_d = 10{,}000$ was used for the comparison of the result of Eq. (15), represented as the bold line. The zero damping rates, obtained from the homogeneous linear equation for the analytical model without the accumulator, are plotted as the open symbols. The boundaries of cavitation surge obtained from the present results with $l_d = 10{,}000$ are the perfect agreement with the result of Eq. (15). The upper and lower regions of the open symbols indicate the stable and unstable regions of cavitation surge, respectively. The result shows that the onset condition of cavitation surge indicates the positive slope. That is, the increase of the cavitation compliance has the stabilizing effect and the increase of the mass flow gain factor causes cavitation surge. For $l_u = 10$, point A is located in the cavitation surge region. On the other

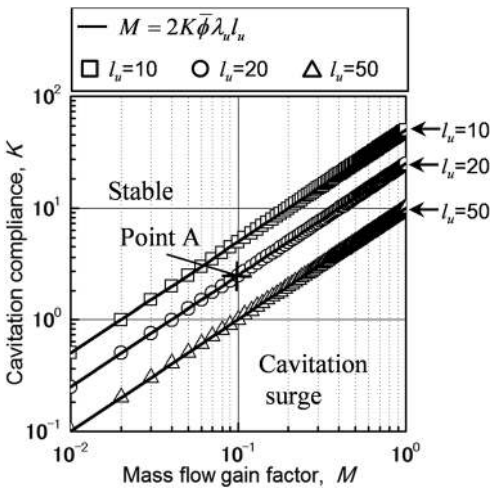

Fig. 4 Stability map for various inlet pipe lengths with $l_d = 10{,}000$

hand, for $l_u = 50$, point A is located in the stable region. This indicates that the longer inlet pipe length has the stabilizing effect.

Figure 5 shows the angular frequencies at the onset boundary of cavitation surge shown in Fig. 4, against the cavitation compliance for various inlet pipe lengths. The horizontal and vertical axes represent the cavitation compliance and the angular frequency, respectively. The open symbols indicate the present results and the bold line represents the result of Eq. (16). All results are completely the same as the result of Eq. (16). The angular frequency of cavitation surge is identical to the resonance frequency of the hydraulic system. The inlet pipe length and the reciprocal of the cavitation compliance correspond to the fluid mass and the spring element, respectively. Thus, the angular frequency of cavitation surge is reduced with the increases of the inlet pipe length and the cavitation compliance. By the comparison of Eqs. (15) and (16), it can say that the present results have quantitative reliability and validity.

Next, we discuss the energy balance in the hydraulic system. The positive and negative energies mean the supplied energy and the energy loss in the hydraulic system, respectively. If the unsteady work of the hydraulic system for one cycle is positive, the hydraulic system will gain energy from themselves, i.e., this phenomenon is called a self-excited oscillation.

Since the integration of the first-order terms of the unsteady work within a period T is zero, the second-order term of the unsteady work remains. Thus, the unsteady work of the inlet pipe E_1 can be expressed as follows:

$$E_1 = -\int_0^T \mathrm{Re}[\hat{\psi}_u e^{j\omega t}]\mathrm{Re}[\hat{\phi}_u e^{j\omega t}]dt - \lambda_u l_u \bar{\phi}\int_0^T \mathrm{Re}[\hat{\phi}_u e^{j\omega t}]^2 dt \quad (17)$$

Here, the first and second terms of E_1 show the unsteady pressure work and the unsteady viscosity work, respectively. By Eq. (7) with the assumption of $\hat{\phi}_d = 0$, $\hat{\psi}_u$can be written as

$$\hat{\psi}_u = \frac{(1 - j\omega M)}{j\omega 2K}\hat{\phi}_u = \left(-\frac{M}{2K} - \frac{j}{2\omega K}\right)\hat{\phi}_u \quad (18)$$

By putting Eq. (18) in Eq. (17) and by assuming the zero imaginary part of $\hat{\phi}_u$, we can obtain the following equation:

$$E_1 = \left(\frac{M}{2K} - \lambda_u l_u \bar{\phi}\right)\hat{\phi}_u^2 \frac{\pi}{\omega} \quad (19)$$

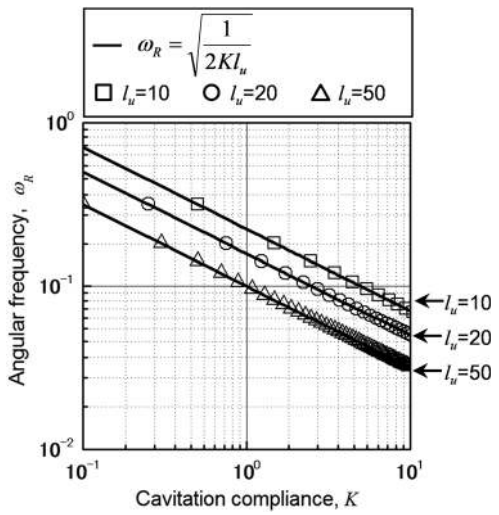

Fig. 5 Angular frequencies for various inlet pipe lengths with $l_d = 10{,}000$

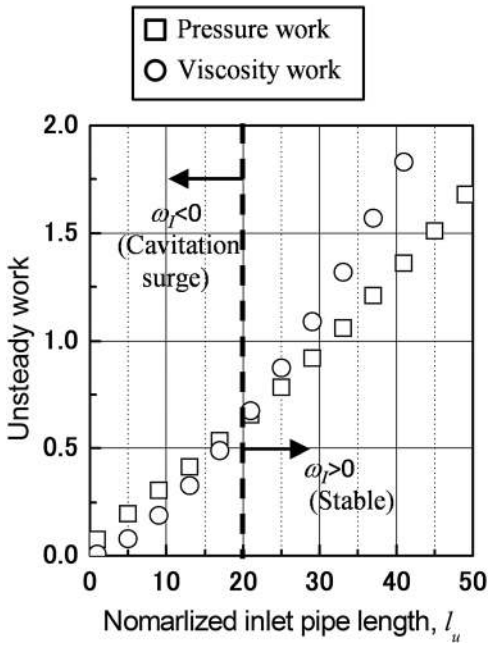

Fig. 6 Unsteady pressure and viscosity works for various inlet pipe lengths with $l_d = 10{,}000$

If E_1 has the positive value, cavitation surge occurs. Thus, cavitation surge occurs in $M > 2K\bar{\phi}\lambda_u l_u$, which is identical to Eq. (15). This result shows that cavitation surge occurs due to the positive mass flow gain factor and the unsteady viscosity work makes cavitation surge stable.

Figure 6 shows the unsteady pressure work and the unsteady viscosity work of E_1 at point A of Fig. 4, calculated by Eq. (17) with the assumption of $\hat{\phi}_u = 1$. The abscissa and ordinate show the inlet pipe length and E_1, respectively. The right and left sides of the dashed line indicates the stable region $\omega_I > 0$ and cavitation surge $\omega_I < 0$. The open symbols show the unsteady pressure work and the unsteady viscosity work. As the inlet pipe length increases, both the unsteady pressure work and the unsteady viscosity work increase. When the unsteady viscosity work is larger than the unsteady pressure work, E_1 has the negative value and then cavitation surge becomes stable. Since the gradient of the viscosity work is expressed as the loss coefficient λ_u and the steady flow coefficient $\bar{\phi}$, the increases of λ_u and $\bar{\phi}$ make cavitation surge stable.

Influence of Outlet Pipe Length. Figure 7 shows the stability map of cavitation surge for various outlet pipe lengths with

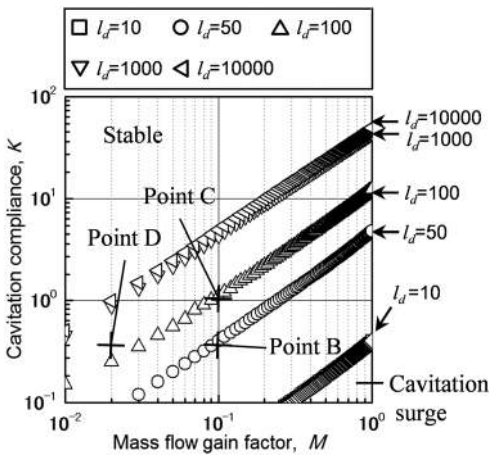

Fig. 7 Stability map for various outlet pipe lengths with $l_u = 10$

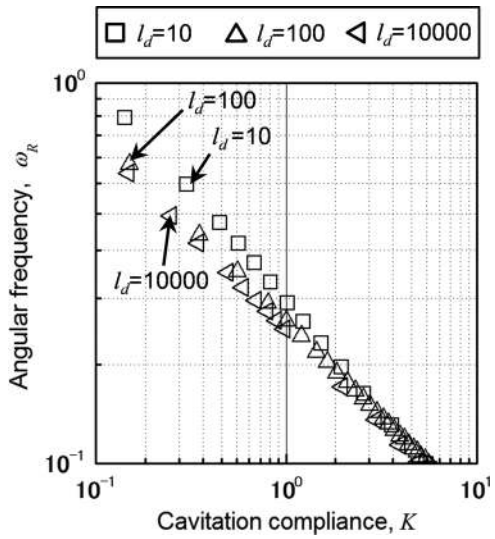

Fig. 8 Angular frequencies for various outlet pipe lengths with $l_u = 10$

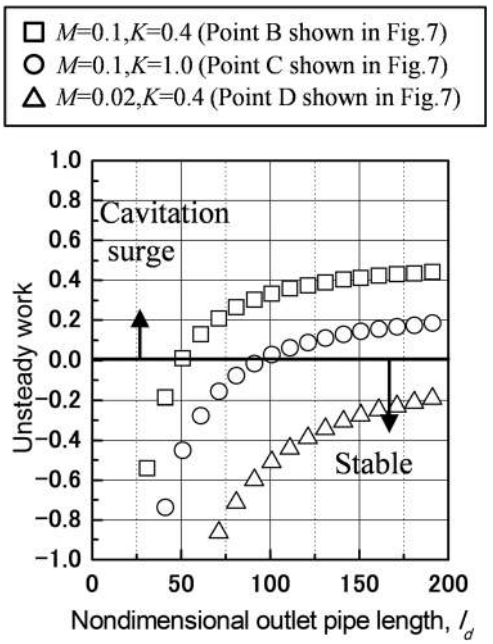

Fig. 10 Unsteady works of the inlet pipe for point B, point C, and point D in Fig. 7

$l_u = 10$. The zero damping rates are plotted as the open symbols. As the outlet pipe length decreases, the stable region is extended toward the bottom. That is, decreasing the outlet pipe length has a stabilizing effect. This stabilizing effect is enhanced at shorter outlet pipe lengths.

Figure 8 shows the angular frequencies at the onset conditions of cavitation surge against cavitation compliance for various outlet pipe lengths. At lower cavitation compliances, the frequency of cavitation surge is slightly increased with the decrease of the outlet pipe length.

Figure 9 indicates the influence of the inlet and outlet loss coefficients on cavitation surge with $l_u = 10$ and $l_d = 100$. The inlet loss coefficient is more effective for the suppression of cavitation surge. This suggests that the inlet valve is more suitable for the suppression of cavitation surge than the outlet valve.

Figure 10 shows the unsteady work of the inlet pipe E_1 at point B, point C, and point D of Fig. 7, calculated by Eq. (17) with the assumption of $\hat{\phi}_u = 1$. The horizontal and vertical axes show the dimensionless outlet pipe length and E_1, respectively. As the outlet pipe length increases, E_1 is increased but converged at a certain value for all cases. The converged unsteady works are decreased with the increase of K and decrease of M. This shows that M causes cavitation surge and K has a stabilizing effect. Moreover, the gradient of E_1 is increased with the decrease of the outlet pipe length. That is, the unsteady work of the inlet pipe is sharply decreased for shorter outlet pipe lengths. This result shows the reason that the stabilizing effect is enhanced at the decrease of the outlet pipe length as shown in Fig. 7.

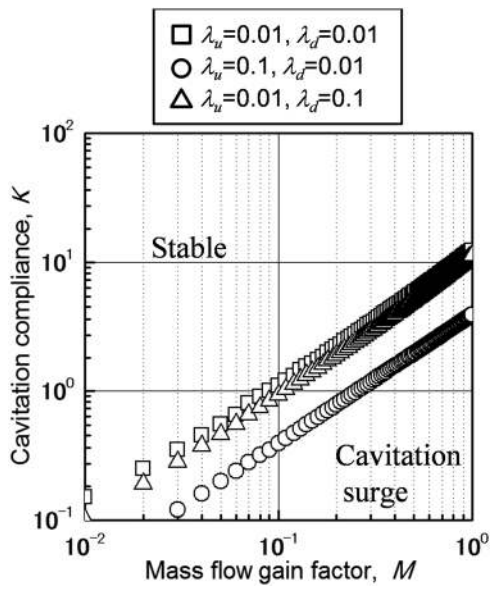

Fig. 9 Influence of the inlet and outlet loss coefficients with $l_u = 10$ and $l_d = 100$

The unsteady energy of the hydraulic system without an accumulator is divided into three parts, which are the unsteady work of the inlet pipe E_1, the unsteady work of the cavitating pump E_2, and the unsteady work of the outlet pipe E_3. The unsteady work of the cavitating pump E_2 can be written as

$$E_2 = \int_0^T \mathrm{Re}[\hat{\psi}_d e^{j\omega t}]\mathrm{Re}[\hat{\phi}_d e^{j\omega t}]dt - \int_0^T \mathrm{Re}[\hat{\psi}_u e^{j\omega t}]\mathrm{Re}[\hat{\phi}_u e^{j\omega t}]dt = E_p + E_c \tag{20}$$

The unsteady work of the cavitating pump E_2 consists of the unsteady pump work

$$E_p = \int_0^T \mathrm{Re}[\hat{\psi}_d e^{j\omega t} - \hat{\psi}_u e^{j\omega t}]\mathrm{Re}[\hat{\phi}_d e^{j\omega t}]dt \tag{21}$$

and the unsteady cavitation work.

$$E_c = \int_0^T \mathrm{Re}[\hat{\psi}_u e^{j\omega t}]dv_c = \int_0^T \mathrm{Re}[\hat{\psi}_u e^{j\omega t}]\frac{dv_c}{dt}dt = \int_0^T \mathrm{Re}[\hat{\psi}_u e^{j\omega t}]\mathrm{Re}[(\hat{\phi}_d e^{j\omega t} - \hat{\phi}_u e^{j\omega t})]dt \tag{22}$$

The unsteady work of the outlet pipe E_3 can be expressed as follows:

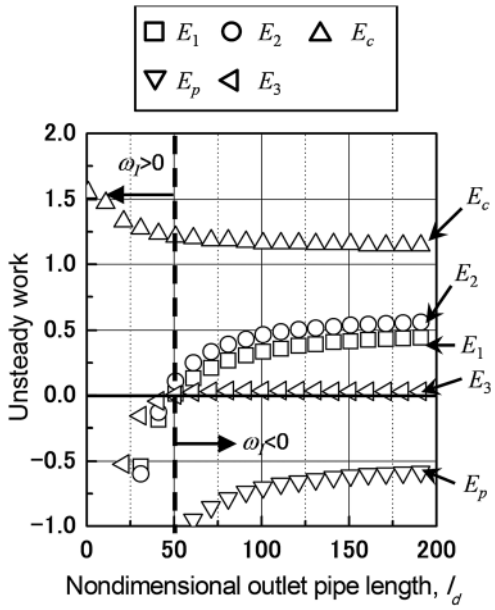

Fig. 11 All unsteady works in the hydraulic system at point B in Fig. 7

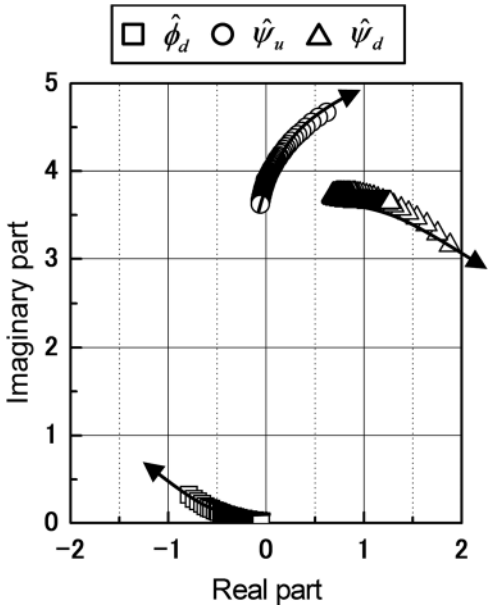

Fig. 12 Complex amplitudes of the unsteady outlet flow and the unsteady inlet and outlet pressures

$$E_3 = \int_0^T \mathrm{Re}[\hat{\psi}_d e^{j\omega t}]\mathrm{Re}[\hat{\phi}_d e^{j\omega t}]dt - \lambda_d l_d \bar{\phi} \int_0^T \mathrm{Re}[\hat{\phi}_d e^{j\omega t}]^2 dt \quad (23)$$

Figure 11 shows the all unsteady works E_1, E_2, E_p, E_c, E_3, at point B of Fig. 7. The horizontal and vertical axes show the dimensionless outlet pipe length and the unsteady works, respectively. Except for E_c, all unsteady works increase with the increase of the outlet pipe. The zero damping rate corresponds to the zero unsteady works of the inlet pipe and the outlet pipe. E_p make cavitation surge stable, and E_c has the destabilizing effect.

Figure 12 shows the complex magnitudes of the unsteady outlet flow and the unsteady inlet and outlet pressures in the complex plane. The outlet pipe length is decreased in the direction of the arrow. The complex magnitude of the unsteady outlet flow is located in the second quadrant and the magnitude of the unsteady outlet flow is increased as the outlet pipe length decreases. The location of the complex magnitude of the unsteady inlet pressure is moved to the second quadrant from the first quadrant as the outlet pipe length decreases. The complex magnitude of the unsteady outlet pressure is located in the first quadrant and the magnitude of the unsteady outlet pressures is increased as the outlet pipe length decreases. These results show that E_1, E_3, E_p are decreased and E_c is increased as the outlet pipe length decreases, expected from Eqs. (17), (21), (22), and (23).

Influence of Accumulator. Figure 13 shows the influence of accumulators on the onset condition of cavitation surge. The closed symbols show the results without the accumulator and the open symbols show the results with the accumulators upstream

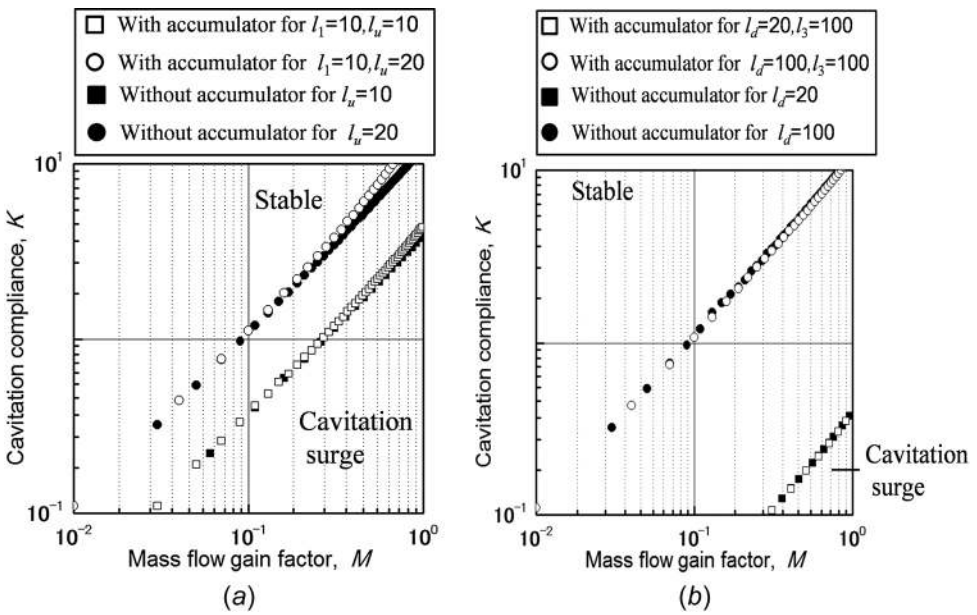

Fig. 13 Influence of the accumulators on the stability map: (*a*) influence of the accumulator upstream of the cavitation pump with $l_d = 10$ and (*b*) influence of the accumulator upstream of the cavitation pump with $l_u = 10$

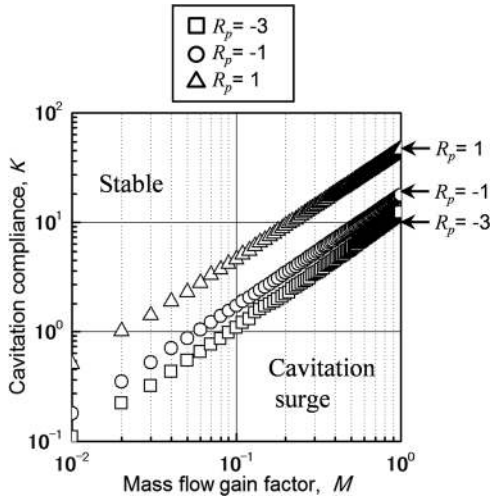

Fig. 14 Influence of flow gain on the stability map

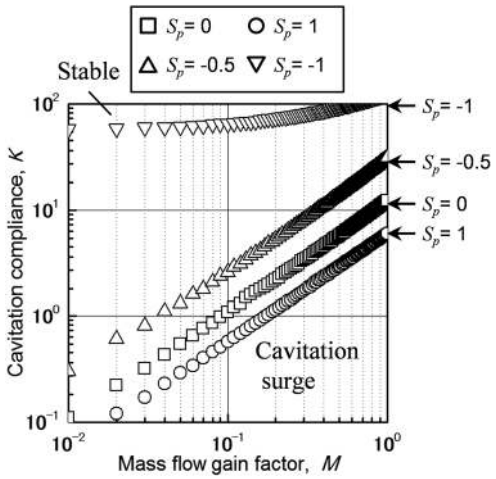

Fig. 16 Influence of pressure gain on the stability map

and downstream of the cavitating pump as shown in Figs. 3(*b*) and 3(*c*). The results with the accumulator upstream of the cavitating pump for $l_u = 10$ and $l_u = 20$ are similar to the results without the accumulator for $l_u = 10$ and $l_u = 20$, as shown in Fig. 13(*a*). In the results with the accumulator downstream of the cavitating pump, the results for $l_d = 20$ and $l_d = 100$ are similar to the results without the accumulator for $l_d = 20$ and $l_d = 100$, as shown in Fig. 13(*b*). These results show that the onset condition of cavitation surge depends on the pipe length between the cavitating pump and the accumulator. Increasing the distance between the upstream accumulator and the cavitating pump enlarged the stable region. On the other hand, decreasing the distance between the downstream accumulator and the cavitating pump enlarged the stable region. The influence of the compliance of the accumulator on the onset condition of cavitation surge was investigated. No significant difference, however, could be observed.

Influence of Flow and Pressure Gains of Cavitating Pump. Figure 14 shows the influence of flow gain on the onset condition of cavitation surge for the default parameters shown in Table 1, with the zero gradient of the suction performance curve $S_p = 0$. The region of cavitation surge is widened with the increase of flow gain. This suggests that the positive flow gain causes cavitation surge called as choke surge.

Figure 15 shows the damping rates of cavitation surge ω_{1I} and the divergence solution ω_{3I} at point B and point C shown in Fig. 7. The horizontal and vertical axes show flow gain and the damping rates, respectively. The damping rates of cavitation surge ω_{1I} are represented by the open symbols, and the divergence solution ω_{3I} are plotted by the closed symbols. The divergence solution ω_{3I} does not depend on the cavitation compliance. It can be considered that the divergence solution is closely related to the onset condition of normal surge. As flow gain is increased, both the damping rates of cavitation surge ω_{1I} and the divergence solution ω_{3I} are decreased. That is, the increase of flow gain causes not only normal surge but also cavitation surge. If flow gain was increased due to cavitation, for $K = 1$, cavitation surge occurs before normal surge.

Figure 16 shows the influence of pressure gain on the onset condition of cavitation surge for the default parameters shown in Table 1 with the negative gradient of the pressure performance curve $R_p = -3$. The region of cavitation surge is suddenly widened for $S_p = -1.0$. This shows that the negative pressure gain leads to cavitation surge.

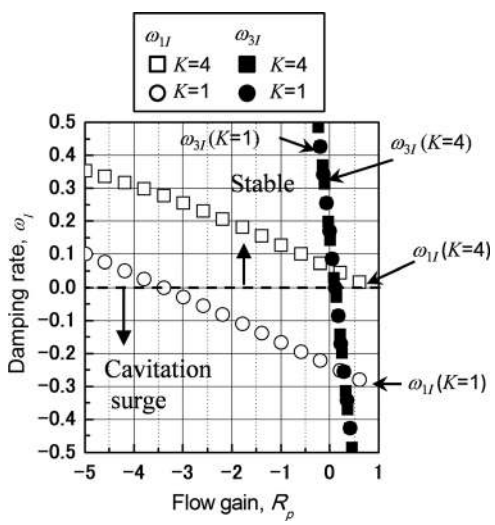

Fig. 15 Damping rates of cavitation surge and normal surge for flow gains at point B and point C shown in Fig. 7

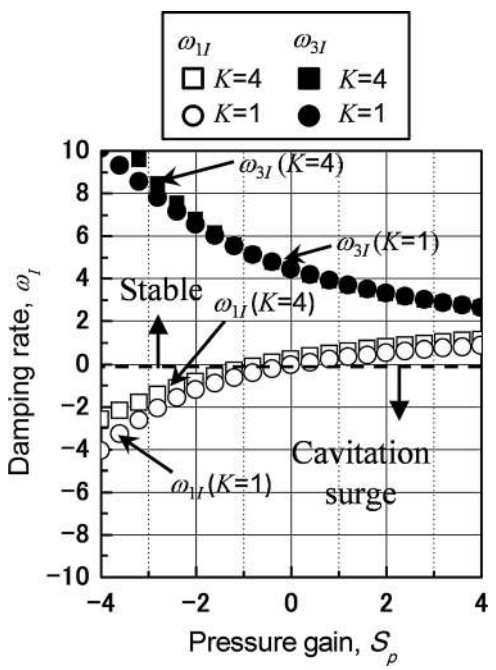

Fig. 17 Damping rates of cavitation surge and normal surge for flow gains at point B and point C shown in Fig. 7

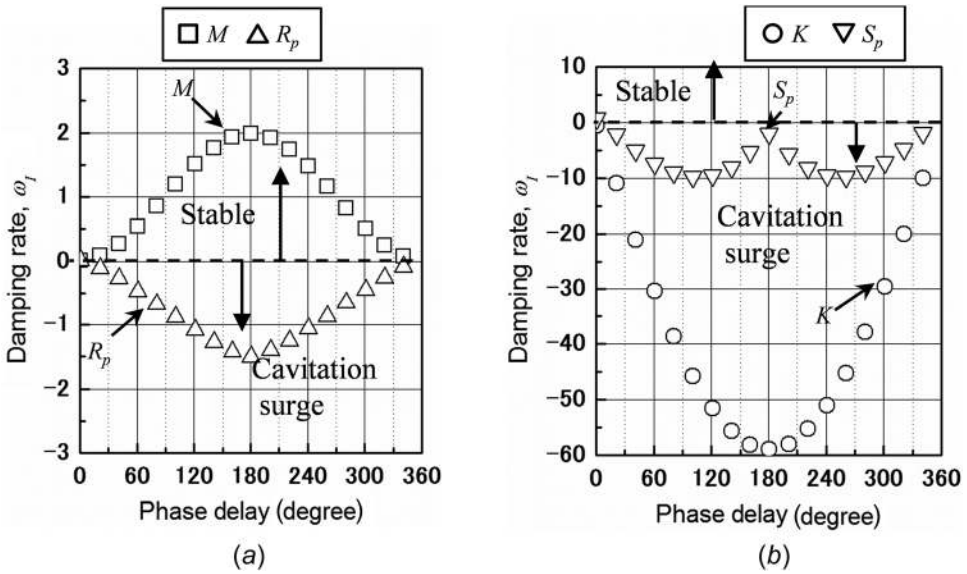

Fig. 18 Damping rates for the phase delay of M, R_p, K, and S_p to the inlet flow oscillation with $l_u = 10$, $l_d = 50$

Figure 17 shows the damping rates of cavitation surge ω_{1I} and the divergence solution ω_{3I} at point B and point C shown in Fig. 7. The damping rates of cavitation surge ω_{1I} are represented by the open symbols and the divergence solutions ω_{3I} are plotted as the closed symbols. As pressure gain decreases, the damping rates of cavitation surge and the divergence solutions are decreased and increased, respectively. This result shows that the decrease of pressure gain causes cavitation surge but not normal surge.

Influence of Unsteady Effect. In order to investigate the influences of the unsteady performance curves and the unsteady cavitation characteristics, R_p, S_p, M and K are expressed as the complex number as follows:

$$R_p = \tilde{R}_p e^{i\alpha}, S_p = \tilde{S}_p e^{i\alpha}, M = \tilde{M} e^{i\alpha}, K = \tilde{K} e^{i\alpha} \tag{24}$$

Here, α is the phase delay to the inlet flow rate oscillation.

Figure 18 shows the damping rates of cavitation surge ω_{1I} for the phase delay of M, R_p, K, and S_p to the inlet flow oscillation, at point B shown in Fig. 7. For M, K, and R_p, the damping rates of cavitation surge ω_{1I} were evaluated with the amplitudes $\tilde{M} = 0.1$, $\tilde{R}_p = -3$, $\tilde{K} = 0.4$, and $\tilde{S}_p = 0$. In order to investigate the influence of S_p, the amplitude $\tilde{S}_p = 1$ was used. At the phase delay of 180 deg, M has the maximum damping rate and both K and R_p have the minimum damping rates. On the other hand, S_p has the minimum damping rate at the phase delay of 90 deg. This means that the onset of cavitation surge is closely related to the real parts of M, K, and R_p and the imaginary part of S_p.

Conclusion

The influences of the hydraulic system on cavitation surge based on the one-dimensional linear stability analysis by the lump-parameter models were investigated. The following conclusions are obtained:

(1) The relative long inlet pipe and short outlet pipe have a stabilizing effect.
(2) The inlet loss coefficient is more effective for the suppression of cavitation surge. This suggests that the inlet valve is more suitable for the suppression of cavitation surge than the outlet valve.
(3) The onset condition of cavitation surge depends on the pipe length between the cavitating pump and the accumulator. This suggests that the accumulator downstream of the cavitating pump has the stabilizing effect.
(4) The negative gradient of the suction performance curve and the positive gradient of the pressure performance curve cause cavitation surge.
(5) The real parts of M, K, and R_p and the imaginary part of S_p are closely related to the onset condition of cavitation surge.

Acknowledgment

The authors would like to thank Professor Watanabe of Kyusyu University who gave productive comments for this study and Professor Tsujimoto of Osaka University who offered useful suggestions to make this study more valuable. This study was made under the support of Grant-in-Aid of EBARA corporation.

Nomenclature

A = area of pipe (m^2)
c = compliance of tank, defined by Eq. (4)
D = diameter of pipe (m)
E_c = cavitation work, defined by Eq. (22)
E_p = unsteady pump work, defined by Eq. (21)
E_1 = unsteady work upstream of the cavitating pump, defined by Eq. (19)
E_2 = unsteady work between the cavitating pump, defined by Eq. (20)
E_3 = unsteady work downstream of the cavitating pump, defined by Eq. (23)
j = imaginary unit in time
K = cavitation compliance, defined by Eq. (6)
l = dimensionless length of pipe
L = length of pipe (m)
M = mass flow gain factor, defined by Eq. (6)
p = pressure (N/m^2)
Q = volume flow rate (m^3/s)
R_p = flow gain, defined by Eq. (10)
S_p = pressure gain, defined by Eq. (10)
t = dimensionless time
T = period of the oscillation
U = tip velocity of a impeller (m/s)
v_a = dimensionless fluid volume at the top of the accumulator
v_c = dimensionless cavitation volume
V_a = fluid volume at the top of the accumulator (m^3)
V_c = cavitation volume (m^3)

α = phase delay to the inlet flow oscillation (rad)
γ = specific heat ratio
λ = loss coefficient
ρ = density of working fluid (kg/m^3)
σ = cavitation number, $\sigma = 2(p - p_v)/\rho U^2$
τ = time (s)
ϕ = flow rate coefficient
ψ = pressure coefficient
ψ_p = pressure rise supplied from the cavitating pump, defined by Eq. (8)
ω = complex number of angular velocity

Subscripts

d = downstream of the cavitating pump
i = inlet tank
I = imaginary part of the complex number
o = outlet tank
R = real part of the complex number
t = total pressure
u = upstream of the cavitating pump
v = vapor pressure
1 = inlet pipe
2 = cavitating pump
3 = outlet pipe

Superscripts

$\hat{}$ = complex number of unsteady component
$\bar{}$ = steady component
$\tilde{}$ = real amplitude of unsteady component

References

[1] Acosta, A. J., 1958, "An Experimental Study of Cavitating Inducers," Proceeding of the 2nd Symposium on Naval Hydrodynamics, Paper No. ONR/AVR-38, pp. 533–557.
[2] Tsujimoto, Y., Yoshida, Y., Maekawa, Y., Watanabe, S., and Hashimoto, T., 1997, "Observations of Oscillating Cavitation of an Inducer," ASME J. Fluid Eng., **119**, pp. 775–781.
[3] Young, W. E., 1972, "Study of Cavitating Inducer Instabilities, Final Report," Report No. NASA-CR-123939.
[4] Brennen, C. E., and Acosta, A. J., 1976, "The Dynamic Transfer Function for Cavitating Inducer," ASME J. Fluid Eng., **98**, pp. 182–191.
[5] Brennen, C. E., 1978, "The Bubbly Flow Model for the Dynamic Characteristics of Cavitating Pump," J. Fluid Mech., **89**, pp. 223–240.
[6] Tsujimoto, Y., Horiguchi, H., and Yonezawa, K., 2010, "Cavitation Instabilities in Turbopump Inducers," Int. J. Fluid Mach. Syst., **3**, pp. 170–180.
[7] Watanabe, T., Kang, D., Cervone, A., Kawata, Y., and Tsujimoto, Y., 2008, "Choked Surge in a Cavitating Turbopump Inducer," Int. J. Fluid Mach. Syst., **1**, pp. 64–75.
[8] Ng, S. L., and Brennen, C. E., 1978, "Experiments on the Dynamic Behavior of Cavitating Pumps," ASME J. Fluid Eng., **100**, pp. 166–176.
[9] Yamamoto, K., 1990, "Instability in a Cavitating Centrifugal Pump (1st Report, Classification of Instability Phenomena & Vibration Characteristics)," JSME, Ser. B, **56**(523), pp. 82–89 (in Japanese).
[10] Yamamoto, K., and Tsujimoto, Y., 2009, "Backflow Vortex Cavitation and Its Effects on Cavitation Instabilities," Int. J. Fluid Mach. Syst., **2**, pp. 40–54.
[11] Kawata, Y., Tanaka, T., Yasuda, O., and Takeuchi, T., 1988, "Measurement of the Transfer Matrix of a Prototype Multi-Stage Centrifugal Pump," ImechE Paper No. C346/88.
[12] Otsuka, S., Tsujimoto, Y., Kamijo, K., and Furuya, O., 1996, "Frequency Dependence of Mass Flow Gain Factor and Cavitation Compliance of Cavitating Inducer," J. Fluid Mech., **118**, pp. 400–408.
[13] Watanabe, S., Sato, K., Tsujimoto, Y., and Kamijo, K., 1999 "Analysis of Rotating Cavitation in a Finite Pitch Cascade Using a Closed Cavity Model and a Singularity Method," J. Fluid Mech., **121**, pp. 834–840.
[14] Rubin, S., 2004, "An Interpretation of Transfer Function Data for a Cavitating Pump," Proceedings of the 40th AIAA/ASME/SAE/ASEE Joint Propulsion Conference, Paper No. AIAA-2004-4025.
[15] Rubin, S., 1966, "Longitudinal Instability of Liquid Rockets Due to Propulsion Feedback (POGO)," J. Spacecr., **3**(8), pp. 1188–1195.
[16] Tsujimoto, Y., Kamijo, K., and Brennen, C. E., 2001, "Unified Treatments of Instabilities of Turbomachines," AIAA J. Propul. Power, **117**, pp. 636–643.
[17] Yonezawa, K., Aono, J., Kang, D., Horiguchi, H., Kawata, Y., and Tsujimoto, Y., 2012, "Numerical Evaluation of Dynamic Transfer Matrix and Unsteady Cavitation Characteristics of an Inducer," Int. J. Fluid Mach. Syst., **5**(3), pp. 126–133.
[18] Cervone, A., Tsujimoto, Y., and Kawata, Y., 2009, "Evaluation of the Dynamic Transfer Matrix of Cavitating Inducer by Means of a Simplified 'Lumped-Parameter' Model," ASME J. Fluid Mech., **131**(4), p. 041103.